Commun Nonlinear Sci Numer Simulat 19 (2014) 967–976

Contents lists available at ScienceDirect

Commun Nonlinear Sci Numer Simulat

journal homepage: www.elsevier.com/locate/cnsns

Laminar length and characteristic relation in Type-I intermittency

Ezequiel del Rio [a,*], Sergio Elaskar [b], Jose M. Donoso [a]

[a] Dpto. Física Aplicada, ETSI Aeronáuticos, Universidad Politécnica de Madrid, Plaza Cardenal Cisneros 3, 28040 Madrid, Spain
[b] Dpto. de Aeronáutica, Facultad de Ciencias Exactas, Físicas y Naturales, Universidad Nacional de Córdoba, Avenida Vélez Sarfield, 1611, 5000 Córdoba, Argentina

ARTICLE INFO

Article history:
Received 10 January 2013
Received in revised form 24 June 2013
Accepted 14 August 2013
Available online 24 August 2013

Keywords:
Chaos
Intermittency
One dimensional map

ABSTRACT

A method to investigate systems showing Type-I intermittency phenomenon is presented. This method is an extension of the procedure we have recently established to study the Type-II and Type-III intermittencies. With this approach, new accurate analytical expressions for the reinjection and the laminar phase length probability densities are obtained. The new theoretical formulas are tested by numerical computation, showing an excellent agreement between analytical models and numerical results. In addition, our method fully generalizes the well-known classical characteristic relations, in such a way that it properly characterizes those systems showing Type-I intermittency.

1. Introduction

The intermittency phenomenon in chaotic dynamics theory is understood as a specific route to the deterministic chaos when spontaneous transitions between laminar and chaotic dynamics occur. The concept of intermittency was firstly introduced by Pomeau and Maneville in the context of the Lorenz system [1,2], but this way to chaos arises in a great variety of systems, such as in periodically forced nonlinear oscillators, Rayleigh–Bénard convection, derivative nonlinear Schrödinger equation and in the turbulent evolution in hydrodynamics and plasmas [3–7]. The intermittency phenomena are usually classified into three categories, named Type- I, Type-II and Type-III intermittencies, following [8]. To clarify and properly analyze each kind of intermittency, it is useful to employ a set of characteristic parameters which not only allow for the assorting of the intermittency, but also permit to study those problems having partially unknown governing equations, as usually happens in medicine and economics science, for instance [9,10].

The local laminar dynamic of Type-II and Type-III intermittencies evolves around a fixed point of its Poincare map, whereas the laminar behavior of Type I intermittency rises in a narrow channel determined by the local Poincare map in the form:

$$x_{n+1} = \epsilon + x_n + a x_n^p \tag{1}$$

where $a > 0$ accounts for the weight of the nonlinear component and ε is a controlling parameter ($\varepsilon \ll 1$). In some pioneer papers devoted to Type-I intermittency, the nonlinear component is quadratic, (i.e. $p = 2$) but actually this restriction is not necessary. We have consider for the present work even p. In any case, for $\varepsilon > 0$, there is not a fixed point at $x = 0$, and hence, the trajectories slowly move along the narrow channel formed with the bisecting line.

Another characteristic property of the intermittency is the *global reinjection mechanism* that maps trajectories of the system from the chaotic region back into the *local* laminar phase. This mechanism can be described by the corresponding

* Corresponding author. Tel.: +34 913366640; fax: +34 913366303.
E-mail address: ezequiel.delrio@upm.es (E. del Rio).

1007-5704/$ - see front matter © 2013 Elsevier B.V. All rights reserved.
http://dx.doi.org/10.1016/j.cnsns.2013.08.012

reinjection probability density (RPD), which is specified by the chaotic dynamics of the system. The RPD function describes the probability density of the reinjected points into the laminar zone coming from the chaotic one. For the map dealt in Section 4, this mechanism is displayed by the green arrows in Fig. 3. Although the importance of the RPD function in describing the intermittency, analytical expressions for the RPD are available for a very few problems. Therefore, in order to describe the main statistical properties of the trajectories, different approximations for the RPD have been used. In this sense we mention that the most common approach for this probability density is the so-called uniform RPD, which only works for some particular cases [11,12].

From the mathematical RPD shape for each case it is possible to analytically estimate the fundamental characteristic of the intermittency, the probability density of the length of laminar phase $\psi(l)$, depending on l, that approximates the number of iterations in the laminar region, i.e. the length of the laminar phase. Note that the function $\psi(l)$ can be estimated from time series, as it is usual to characterize the intermittency type. The characteristic exponent β, depending on $\psi(l)$, defined through the relation $\bar{l} \propto \varepsilon^{-\beta}$, is also a good indicator of the intermittency type.

In [13], three functions for the RPD corresponding to several choices of the logistic maps were proposed: a uniform RPD, the reinjection in a given point and a nonuniform RPD in the form $\phi(x) \propto (x-\hat{x})^{1/2}$, where $\hat{x}$ is the lower boundary reinjection point (LBR). In [14] it was studied the dependence of the characteristic exponent on the RPD. In this approach the author took as input for the local Poincare map Eq. (1) the more general RPD $\phi(x) \propto (x-\hat{x})^{\alpha}$ for $-1 < \alpha < 0$ where for $\hat{x} = 0$, the characteristic exponent ranged as $0 \leq \beta \leq (p+\alpha-2)/p$. For the case of $p = 2$, only some particular values of the exponent α have been reported for system based on a logistic map. As far as we know, all of the extensions and generalizations given up to now for the RPD render a quantitative but not qualitative change in the shape of ψ. Nowadays, the classical equation for ψ is still in use (see Eq. 3.15 of [15], for instance) to characterize the Type-I intermittency phenomenon, as can also be seen in [16].

Recently, to describe the reinjection mechanisms of a wide class of 1D maps with intermittency of Types II and III, we have addressed in [17,18] the corresponding RPD as generalizations of the cases with $\phi(x) \propto x^{\alpha}$, when only the restriction $-1 < \alpha$ is imposed, including the interesting case of positive α. It was shown that the shape of the RPD is ascertained by the behavior of trajectories within chaotic regime in a neighborhood of a point where the Poincare map has infinite or zero tangent. This tangent determines the sign of the exponent α in the power law assumed in the RPD expression. It has been also shown that this mechanism is robust against the external noise [19].

In the present work, we look deeper into our mentioned approach in order to apply and extend it to the study of Type I intermittency. As a consequence of this generalization for the RPD, we show that the classical shape for ψ associated to Type-I intermittency (see Eq. 3.15 of [15]) can qualitatively change. This interesting fact will be important to characterize some Type-I intermittency scenarios that can have been hidden until today. The new RPD we propose here for Type-I intermittency also covers the well-known classical characteristic relation $\varepsilon^{-\beta}$ where the characteristic exponent β lies in the interval $[0,1]$.

The paper is structured as follows. In Section 2 we describe the theoretical framework, that accounts for a wide class of dynamical systems with Type-II and Type-III intermittencies in order to arrange the extension of the method to the present case. Section 3 is devoted to establish the new analytical probability density of the laminar length based on the RPD. As a consequence, we propose in Section 4 the new characteristic relations for Type-I intermittency and the classical relations that can be considered as particular cases of the new ones. All of the analytical results are confirmed by numerical simulations, as explained in Section 5. The last section is devoted to summarize the conclusions.

2. Assessment of RPD function

To start with our discussion, we briefly describe in this section the theoretical framework we have established in previous works for a wide class of dynamical systems presenting intermittency, with general 1-D map in the form

$$x_{n+1} = F(x_n), \quad F : \mathbb{R} \to \mathbb{R} \tag{2}$$

Our main task is to establish the RPD function, $\phi(x)$, which determines the statistical behavior of system trajectories for each particular shape of $F(x)$. The function $\phi(x)$ can be directly derived from Eq. (2) by meas of the Shaw relation [20]. However, there is no direct and general procedure to obtain accurately its mathematical form from experimental or numerical data, specially when very few data are available. Recently, we have shown that the key point to solve the problem of finding $\phi(x)$ is to determine from time series the integral characteristics

$$M(x) = \begin{cases} \dfrac{\int_{x_s}^{x} \tau\,\phi(\tau)\,d\tau}{\int_{x_s}^{x} \phi(\tau)\,d\tau} & \text{if } \int_{x_s}^{x} \phi(\tau)d\tau \neq 0 \\ 0 & \text{otherwise} \end{cases} \tag{3}$$

where $x_s = x_0 - c$, being $c > 0$ a constant that limits the laminar zone of the intermittency. For this function, we can define the domain of M, i.e. $M : [x_0 - c, c + x_0] \to \mathbb{R}$, where x_0 is the fixed point in the laminar zone of the map (2) for $\varepsilon = 0$. Since $M(x)$ only involves integrals of ϕ, it can be better estimated than ϕ itself, because of the statistical fluctuations are reduced for the cases of having a few data set or for system with high level of noise. To numerically approximate $M(x)$, we notice that it is an average over all reinjection points lying on the interval $(\hat{x}, c + x_0)$, so, we can deal with the approximation

$$M(x) \approx \frac{1}{n}\sum_{j=1}^{n} x_j, \quad x_{n-1} < x \le x_n. \tag{4}$$

Here the reinjection points $\{x_j\}_{j=1}^{N}$ have been sorted as $x_j \le x_{j+1}$ and the lower boundary of reinjections (LBR) approaches $\hat{x} = \inf\{|x_j|\}$ because the LBR indicates the limit value for reinjected points. In the Fig. 3 are represented the two LBRs corresponding to the two reinjected mechanisms shown in this figure. In our previous works we found that for a wide class of maps showing Type-II (and Type-III) intermittency, $M(x)$ follows the linear law

$$M(x) = \begin{cases} m(x-\hat{x}) + \hat{x} & \text{if } x \ge \hat{x} \\ 0 & \text{otherwise} \end{cases} \tag{5}$$

where $m \in (0,1)$ is a free parameter. By means of (3) the corresponding RPD becomes

$$\phi(x) = b(x-\hat{x})^{\alpha}, \quad \text{with} \quad \alpha = \frac{2m-1}{1-m}. \tag{6}$$

where $b = (\alpha+1)/(c-\hat{x})^{(}\alpha+1)$ and, since $m \in (0,1)$, we have $\alpha \in (-1,\infty)$. Observe that for $m = 1/2$, we recover the most common approach of assuming the uniform RPD, $\phi(x) = 1/(c-\hat{x})$. Furthermore, from (6), the two limit cases

$$\phi_0(x) = \lim_{m\to 0} \phi(x) = \delta(x-\hat{x}) \tag{7}$$

$$\phi_1(x) = \lim_{m\to 1} \phi(x) = \delta(x-c) \tag{8}$$

can be also derived for the case of Eq. (7) corresponding to $\alpha \to -1$ and Eq. (8) means that all the points are reinjected on $\hat{x}$.

3. Length of laminar phase

Another fundamental quantity to characterize the intermittency phenomenon is the probability density of the laminar length $\psi(l)$, which depends on the particular form of the RPD and on the number of iterations l in the laminar region. We estimate l by considering, as usual, the approximation of the particular map (1) for the local dynamics by the differential equation [8]

$$\frac{dx}{dl} = \varepsilon + a x^p, \tag{9}$$

from which we obtain $l = L$ as a function of x

$$L(x,c) = \frac{c}{\varepsilon}\,{}_2F_1\left(\frac{1}{p}, 1; 1+\frac{1}{p}; -\frac{ac}{\varepsilon}\right) - \frac{x}{\varepsilon}\,{}_2F_1\left(\frac{1}{p}, 1; 1+\frac{1}{p}; -\frac{ax}{\varepsilon}\right) \tag{10}$$

in terms of the Gauss hypergeometric function ${}_2F_1$(a,b;c;z) [21]. The function $L(x,c)$ is referred to a local behavior, and is controlled by the parameters a, p and ε, of the local map in the neighborhood of the unstable point. The probability of finding a laminar phase of a given length between l and $l + dl$ is $\psi_l(l)dl$, being the density $\psi(l)$

$$\psi(l) = \phi(X(l,c))\left|\frac{dX(l,c)}{dl}\right| = \phi(X(l,c))\left|aX(l,c)^p + \varepsilon\right| \tag{11}$$

where $X(l,c)$ is the inverse of $L(x,c)$ with respect to its first argument. We point out that the function $X(l,c)$ can be explicitly written for a very few cases as, for instance, the corresponding for $p = 2$. However, in all cases, ψ (depending on the parameters a p and α) can be plotted by using the parametrisation

$$(L(x,c), \psi'(x)) = (L(x,c), \phi(x)|\varepsilon + ax^p|). \tag{12}$$

where instead of l we have taken the coordinate of the reinjected points x as the free parameter. According to Eq. (12), the value of $\psi(l)$ for $l = 0$ coincides with $\psi'(x)$ for $x = c$, that is, $\phi(c)(\varepsilon + ac^p)$, this gives for the limit for the maximum length $l = l_{max}$,

$$\lim_{l\to l_{max}} \psi(l) = \lim_{x\to\hat{x}} \psi'(x) = \begin{cases} 0 & \text{if } \alpha > 0 \\ b(\varepsilon + a\hat{x}^p) & \text{if } \alpha = 0 \\ \infty & \text{if } \alpha < 0 \end{cases} \tag{13}$$

which depends on α. It is interesting to observe that if $\alpha > 0$ we have $\psi(l_{max}) = 0$ and the graph for this function is very different from the obtained for the classical $\psi(l)$ that can be seen in [8,15,16], for instance.

The extreme points of the function $\psi(l)$ can be obtained, taking into account Eqs. (9) and (11), from

$$\frac{d\psi(l)}{dl} = \left((\varepsilon + ax^p)\frac{d\phi(x)}{dx} + ap\,\phi(x)x^{p-1}\right)\left|\frac{dX(l)}{dl}\right| = 0 \tag{14}$$

which can be cast into

$$\frac{\mathrm{d}\psi(l)}{\mathrm{d}l} = b(x-\hat{x})^{(\alpha-1)}\left[(\alpha+p)ax^p - ap\hat{x}x^{p-1} + \alpha\varepsilon\right]\left|\frac{\mathrm{d}X(l)}{\mathrm{d}l}\right| = 0. \tag{15}$$

by means of Eq. (6). Since Eq. (9) imposes $\mathrm{d}X(l)/\mathrm{d}l \neq 0$ for $\varepsilon \neq 0$, the expression between the square brackets in Eq. (15) must be zero for $x \in (\hat{x}, c)$ and $\varepsilon \approx 0$, the roots can be finally approximated as

$$x_{r1} \approx 0 \quad \text{and} \quad x_{r2} \approx \frac{p\hat{x}}{\alpha+p}. \tag{16}$$

These estimated values show that the density $\psi(l)$ extrema can occur at two points, $L(x_{r1})$ and $L(x_{r2})$, provided that x_{r1} and x_{r2} lie in $(\hat{x}, c)$. The Table 1 shows all possibilities matching this restriction for both roots. Some laminar length density function shapes are plotted in Fig. 1 showing the dependence on the extreme points, according to the cases referred in Table 1. As said before, the functions depicted in Fig. 1(a), (b) and (f) notably differ from the typical well-known behavior obtained in the classical cases (e.g. see the table of [8]). For the case Fig. 1(b) we also have $\psi(l_{max}) = 0$, but now $\psi(l)$ has a local maximum, what is a remarkable characteristic, as far as we know, never reported for the probability density of the laminar length.

The slope of $\psi(l)$ at the final interval point is determined by the factor $(x-\hat{x})^{(\alpha-1)}$, thus, for $\alpha > 0$ we have

$$\lim_{l\to l_{max}} \frac{\mathrm{d}\psi(l)}{\mathrm{d}l} = \begin{cases} \infty & \text{if } \alpha < 1 \\ (\varepsilon + a\hat{x}^p)^2 & \text{if } \alpha = 1 \\ 0 & \text{if } \alpha > 1 \end{cases} \tag{17}$$

what justifies the rising steeply graphs in the Fig. 1(a) and (b), both built with finite values $0 < \alpha < 1$ to visualize the unbounded slopes analytically provided by Eq. (17). For the particular case $\alpha = 0$ the uniform reinjection expression $\phi(x) = 1/|\hat{x} - c|$ is recovered and from Eq. (15) the exact roots $x_{r1} = 0$ and $x_{r2} = \hat{x}$ hold for any value of ε. Observe that x_{r2} lies on the lower limit of the laminar interval whereas x_{r1} yields to a minimum only if $\hat{x} < 0$.

Table 1
Classification of the $\psi(l)$ local extrema types, minimum (min) or maximum (MAX), at $L(x_{r1})$ and $L(x_{r2})$, according to α and $\hat{x}$ values in the RPD. The limits $\lim_{l\to l_{max}}\psi(l)$, depending on α, are also given. Typical shapes for each case are plotted in subfigures in Fig. 1 as it is specified in the last column.

		$L(x_{r1})$	$L(x_{r2})$	$\lim_{l\to l_{max}}\psi(l)$	Subfigure
$\alpha > 0$	$\hat{x} > 0$	$\nexists$	$\nexists$	0	a
$\alpha > 0$	$\hat{x} < 0$	min	MAX	0	b
$\alpha < 0$	$\hat{x} > 0$	$\nexists$	min	∞	c
$\alpha < 0$	$\hat{x} < 0$	min	$\nexists$	∞	d
$\alpha = 0$	$\hat{x} < 0$	min	$\nexists$	$\frac{\varepsilon+a\hat{x}^p}{\lvert\hat{x}-c\rvert}$	e
$\alpha = 0$	$\hat{x} > 0$	$\nexists$	$\nexists$	$\frac{\varepsilon+a\hat{x}^p}{\lvert\hat{x}-c\rvert}$	f

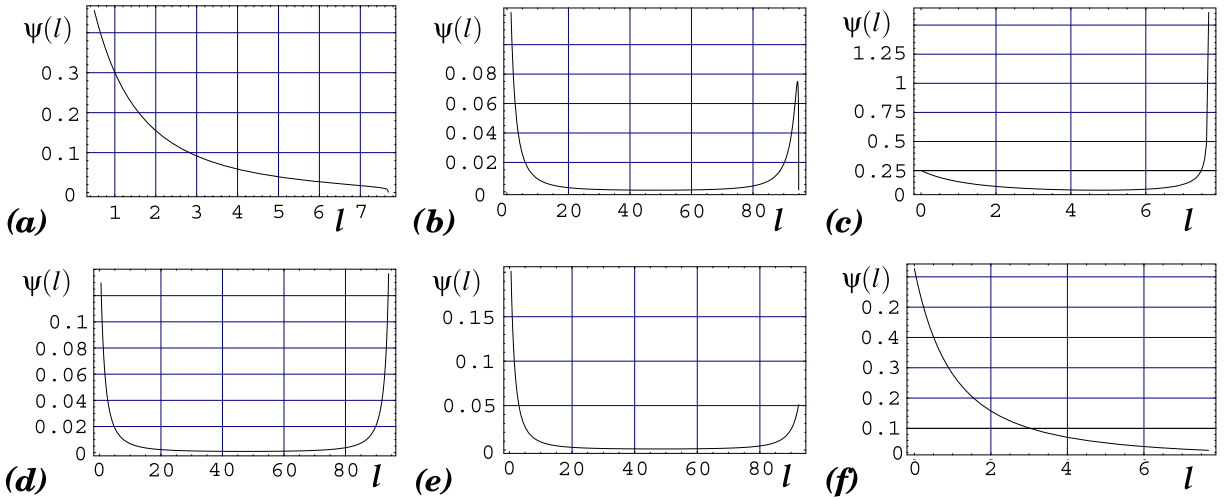

Fig. 1. Different $\psi(l)$ profiles from Eq. (12) as a function of $\hat{x}$ and α. The figures correspond to the parameters of Table 1. The numerical values selected to display the figures are: (a) $\hat{x} = 0.1, \alpha = 0.2$, (b) $\hat{x} = -0.4, \alpha = 0.3$, (c) $\hat{x} = 0.1, \alpha = -0.6$, (d) $\hat{x} = -0.4, \alpha = -0.3$, (e) $\hat{x} = -0.3, \alpha = 0$ and (f) $\hat{x} = 0.1, \alpha = 0$. In all cases $p = 2, a = 1, \varepsilon = 0.001$ and $c = 0.5$.

4. Characteristic relations

Once ψ has been obtained, we are in position to derive the characteristic relations for the Type-I intermittency. First of all, we must analyze the mean value of l given by

$$\bar{l} = \int_0^\infty l\psi(l)\mathrm{d}l. \tag{18}$$

This average $\bar{l}$ is directly related to the characteristic exponent β, commonly used to characterize any type of intermittency, by means of the characteristic relation $\bar{l} \propto \varepsilon^{-\beta}$, which describes, for small values of ε, how the length of the laminar phase increases as ε decreases. Therefore, from Eq. (11), the mean laminar length $\bar{l}$ can be computed by

$$\bar{l} = \int_{\hat{x}}^{c} L(x,c)\phi(x)dx. \tag{19}$$

which, for the case $\hat{x} \approx 0$, and by means of Eqs. (6) and (9), gives

$$\bar{l} = \lim_{x\to 0} \frac{b}{\alpha+1} L(x,c)x^{\alpha+1}\Big|_x^c + \frac{b}{\alpha+1}\int_0^c \frac{x^{\alpha+1}}{\epsilon + ax^p}dx \tag{20}$$

where, for $-1 < \alpha$, the limit in Eq. (20) is zero since ${}_2\mathrm{F}_1(\frac{1}{p}, 1; 1+\frac{1}{p}; 0) = 0$. On the other hand, by replacing in Eq. (20) the parameters α and p by $\alpha - 1$ and $p - 1$ respectively, we recover the integral of the Eq. (12) of our previous work [17]. This fact allows us to directly follow the arguments given in [17] to ensure that the integral of Eq. (20) converges for all α such that $-2 < \alpha < p - 2$. Assuming that α does not depend on ε we obtain

$$\beta = \frac{p-\alpha-2}{p} = 1 - \frac{1}{(1-m)p}. \tag{21}$$

where β here plays the role of $-\beta$ in [17]. Thus, we point out that, in this case, the convergence interval for the integral involved in Eq. (20) is limited by the corresponding values of α for the RPD (i.e. $-1 < \alpha$) what ensures that (21) is a well behaved function for $-1 < \alpha < p - 2$ only, as can be seen in Fig. 2. It is important to stress the fact that Eq. (21) holds not only for $\alpha \leq 0$ but also for $\alpha > 0$. In the classical case, $p = 2$, the expression (21) can be applied only for $\alpha < 0$, that is, only for the decreasing RPD case. However, if the general case is considered, it is possible to get a given characteristic exponent β by combining either RPDs (increasing and decreasing) determined by the parameter α, by suitable elections of p. A numerical verification of this possibility is shown in the following section for $\beta = 1/3$, corresponding to the dashed horizontal line in Fig. 2.

With regard to other values for $\hat{x}$, we should distinguish between two cases, $\hat{x} > 0$ and $\hat{x} < 0$. By virtue of the behavior of the laminar phase length, it can be seen that it increases drastically for those trajectories approaching $x = 0$, a fact that does not happen for $\hat{x} > 0$ where no such kind of trajectories exists. Therefore, in the case of $\hat{x} > 0$, the average laminar length becomes almost independent of ε, so that, we have $\beta = 0$.

The case $\hat{x} < 0$ depends on α as we explain as follows. At this point, having in mind that for $\hat{x} < 0, \alpha$ can be non-zero but the RPD given by Eq. (6) can be locally approximated by the uniform reinjection in the neighborhood of $x = 0$, as in the case of $\alpha = 0$ in [18]. Hence, to derive the characteristic exponent for Type-II and Type-III intermittencies with $\hat{x} < 0$, we can fix $\alpha = 0$ in the corresponding expression for β. However, for this case, there is a substantial difference with respect to the other

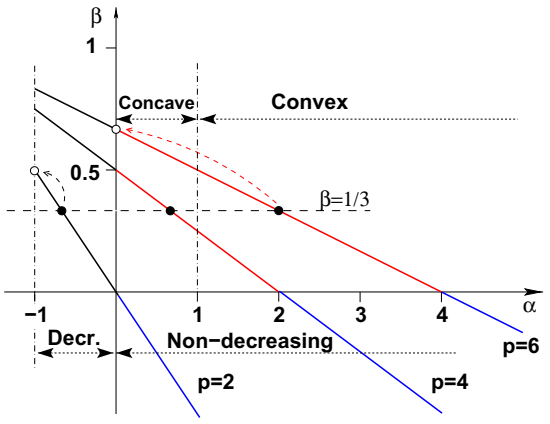

Fig. 2. Characteristic exponent β as a function of α for three particular p according to Eq. (21), valid only for $\beta > 0$ (black and red lines). The RPD decreasing or non-decreasing domains are also indicated. In the last case the two possibilities for the RPD, concave or convex are separated by a vertical line. For $p = 6$ ($p = 2$) the dashed arrow indicates how β given by Eq. (21) approaches the value given by Eqs. (22) and (23) as $\hat{x}$ varies from $\hat{x} = 0$ to negative values. (For interpretation of the references to color in this figure legend, the reader is referred to the web version of this article.)

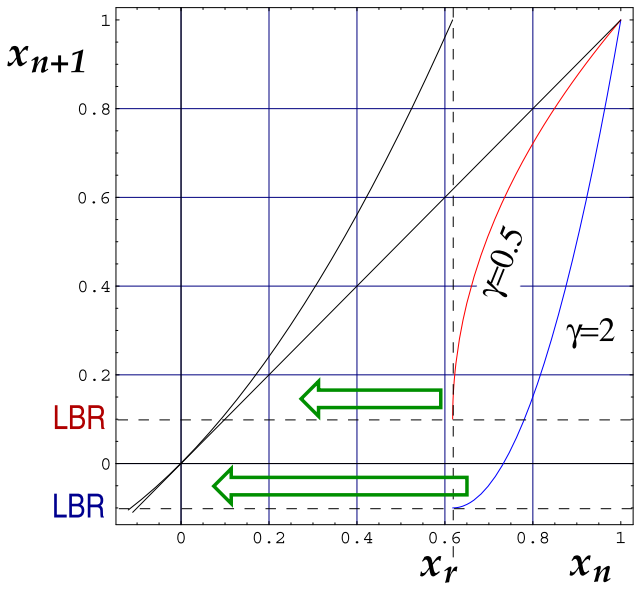

Fig. 3. Map of Eq. (24) for $p = 2$ with the bisecting line. The vertical dashed line indicates x_r. Cases of $\gamma = 0.5$ and $\gamma = 2$ correspond to the red and blue lines, The green arrows indicate the corresponding reinjection mechanism that gives the different RPDs. For each case, the LBRs $\hat{x} = 0.1$ and $\hat{x} = -0.1$ are also indicated. (For interpretation of the references to color in this figure legend, the reader is referred to the web version of this article.)

cases. Whereas in Type-II and Type-III intermittencies the points reinjected far from $x = 0$ do not have a crucial contribution to $\bar{l}$, in Type-I intermittency the reinjected points with $x < 0$ exhibit trajectories passing across the narrow gap along the whole laminar phase. In view of this feature, if the RPD remains very small for $x < 0$, as it is in fact the case of $\alpha > 1$, we still can neglect the contribution on $\bar{l}$ of all those points reinjected with $x < 0$. In other words, we are able to estimate the characteristic exponent by simply setting $\alpha = 0$ in Eq. (21), this leads to

$$\beta = \frac{p-2}{p}, \tag{22}$$

expression that has been verified by the numerical calculations we present in the following section.

It must be emphasized that Eq. (22) differs from the relation proposed in Ref. [14] because in this approach the authors only considered the case $\alpha < 0$, hence most points are reinjected with $x < 0$, so most of the trajectories go through the laminar phase, as it happens in the limit $\alpha \to -1$. Therefore, by setting in Eq. (21) $\alpha = -1$, the relation proposed in Ref. [14]

$$\beta = \frac{p-1}{p} \tag{23}$$

is recovered.

In Fig. 2 a dashed arrow indicates the shifting of the characteristic exponent from corresponding to Eq. (21) marked by bullets, to marks of the open circles corresponding to by Eqs. (22) and (23) for $\alpha > 0$ and $\alpha < 0$ respectively.

5. Numerical simulation

In this section we check and compare the previous analytical results with numerical simulations. Among of great variety of maps showing Type-I intermittency, there is a class of maps for which the local part and the chaotic parts become explicitly separated in its algorithm. For these maps it is relatively simply to control the parameter what makes them suitable to carry on a comparison between analytical and numerical results (see, among others, the maps studied in [11,17,22,23]).

In this sense, to deal with an exemplifying Type-I intermittency behavior, we have modified the map [17] (a generalization of the map used in [11]) as follows

$$x_{n+1} = F(x_n) = \begin{cases} \varepsilon + x_n + a|x_n|^p & \text{if } x_n < x_r \\ (1-\hat{x})\left(\frac{x_n - x_r}{1-x_r}\right)^{\gamma} + \hat{x} & \text{otherwise} \end{cases} \tag{24}$$

where x_r is the root of the equation $\varepsilon + x_n + x_n^p = 1$, $\gamma > 1$ draws the nonlinear term of the reinjection mechanism and the parameter $\hat{x}$ corresponds to the LBR. In Fig. 3 we present the map graphs for different values of the parameters γ and $\hat{x}$.

The method we have presented in this work is applied to study the map Eq. (24). In order to confirm that the function $M(x)$ can be approximated by Eq. (5), we have computed this function by using Eq. (4), the results are shown in Fig. 4 for two values of γ. In this figure, the solid line corresponds to the least mean square fit while dots are referred to the numerical values. As Fig. 4 shows, the approximation provided by Eq. (5) and the numerical data are, in practice, indistinguishable. The RPD is obtained according to Eq. (6) by using the computed values of m and $\hat{x}$ that satisfy $M(\hat{x}) = \hat{x}$. We point out that in this case $\hat{x}$ is a control parameter for the map but, in general, we can find its value by fitting the numerical or experimental data to Eq. (5). In Fig. 5(a) and (b) we have plotted the RPD given by Eq. (6) with $\hat{x}$ and m coming from the numerical data used in Fig. 4.

Concerning the probability density of the laminar phase length $\psi(l)$, the subfigures *c, d* and *e* of Fig. 1 present several shapes very similar to the classical function proposed in [15]. However, the shapes plotted in subfigures *a, b* and *f* are quite different from the classical one. To be concise, we have numerically checked the prediction shown in Fig. 1(a) and (b). In this case a suitable value of γ was necessary to provide a RPD with $\alpha > 0$, an estimation of α as a function of γ was obtained by following Ref. [17], as

$$\alpha \approx \gamma^{-1} - 1. \tag{25}$$

Thus, to obtain a positive α, we require γ less than 1. Therefore the values $\gamma = 0.55$ and $\gamma = 0.7$, together with the values of the $\hat{x}$ used in Fig. 4, constitute a suitable set of parameters to study the case referred in rows *a* and *b* of the Table 1.

In Fig. 5(c) and (d) graphs for the analytical expression Eq. (12) are shown. We have used the same function $\phi(x)$ of Fig. 5(a) and (b) and they have been obtained from the function $M(x)$ used for Fig. 4. The insets in Fig. 5(c) and (d) underline

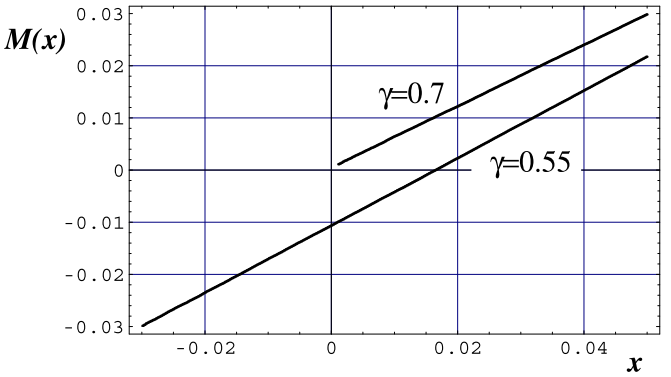

Fig. 4. Dots showing numerical $M(x)$ values from Eq. (4) for the map Eq. (24) and solid lines for the corresponding least mean square fit, they are in practice indistinguishable. The slopes are $m(\gamma = 0.7) = 0.588$ and $m(\gamma = 0.55) = 0.645$ with the parameters: $a = 1, p = 2, c = 0.05, \varepsilon = 10^{-4}$ and $\hat{x} = 0.001$ for $\gamma = 0.7$ and $\hat{x} = -0.03$ for $\gamma = 0.55$.

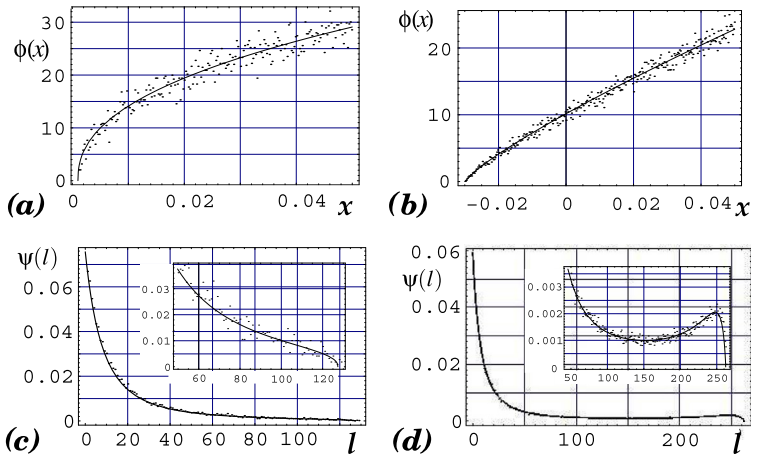

Fig. 5. RPD and $\psi(l)$ for the map Eq. (24) with the same parameters values employed in Fig. 4. Dots correspond to numerical results. To plot the RPDs in the frames (a) and (b), for $\gamma = 0.7$ and $\gamma = 0.55$ respectively, Eq. (6) is used with m obtained by fitting the data of Fig. 4, giving the following values of α. (a): $m = 0.588, \alpha = 0.426$. (b): $m = 0.645, \alpha = 0.824$. The function $\psi(l)$ from Eq. (12) corresponding to the RPDs of (a) and (b) are presented by solid lines in the subfigures (c) and (d) respectively. The insets in (c) and (d) are zoomed images corresponding to the greatest l.

the different behaviors of $\psi(l)$ for the largest values of l. In both cases, he have found an excellent agreement between numerical data (dots) and analytical expressions given by Eq. (12).

Regarding the characteristic relation, we have used Eqs. (21) and (25) to get the relationship between any of the two pairs of parameters p, γ and p', γ' of the map Eq. (24) that lead to the same given characteristic exponent β. Then, if (p, γ) provide a given β the same values can be obtained by with the pair (p', γ') by applying the relation

$$\gamma' = \frac{p\gamma}{(p'-p)\gamma + p'}. \tag{26}$$

In this sense, we proceed by numerically evaluating the exponent β for $p = 2, p = 4$ and $p = 6$. For the first case we chose $\gamma_2 = 3$ for which we have $\beta = 1/3$. For the other case from Eq. (26) we have $\gamma_4 = 3/5$ and $\gamma_6 = 1/5$ for $p = 4$ and $p = 6$ respectively. Fig. 6 shows the characteristic relations for these parameter values. Numerical data are fitted and depicted by the three parallel lines which show that the characteristic exponent β can be approximated in either case by $\beta \approx 0.344$, very close to the analytical expected value $\beta = 1/3$. Each line slope in Fig. 6 corresponds to a bullet of the horizontal dashed line of Fig. 2. Note that we have chosen the three cases as distributed over the three regions labeled in Fig. 2. Note that if only adecreasing RPD functions are considered (then $\alpha < 0$), to get a characteristic exponent in the interval $0 < \beta < 1/2$, it must be $p = 2$, as Eq. (21) establishes. This case is shown by a black solid line in Fig. 6. we have also plotted the red solid lines corresponding to cases also drawn in red color in Fig. 2.

With respect to the characteristic relation for $\hat{x} < 0$, we have set $\hat{x} = -0.05$ in the examples, for $p = 6$ and $p = 4$, as referred in Fig. 6, having $\alpha > 1$ and $0 < \alpha < 1$, respectively. The numerical characteristic relations are plotted in Fig. 7 (dots)

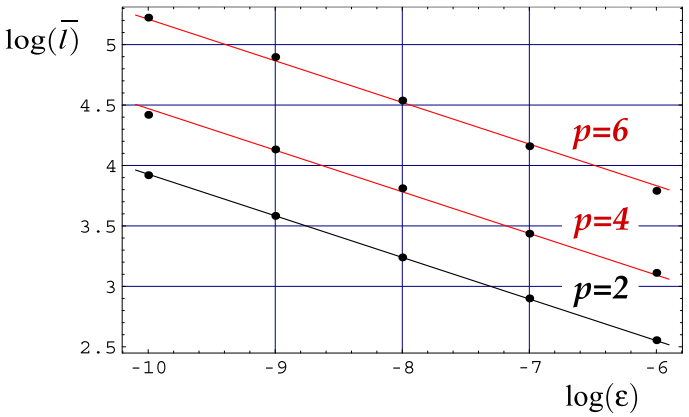

Fig. 6. Characteristic relations for the map (24) for the three p values used in Fig. 2. The exponent γ has been chosen to give the same critical exponent β, according to Eq. (26). Dots stand for the numerical simulation results, the parallel solid lines are fits of the numerical data with $\beta \approx 0.344$, close to the analytical value $\beta = 1/3$. In all cases $a = 1, \hat{x} = 0$ and $c = 0.05$.

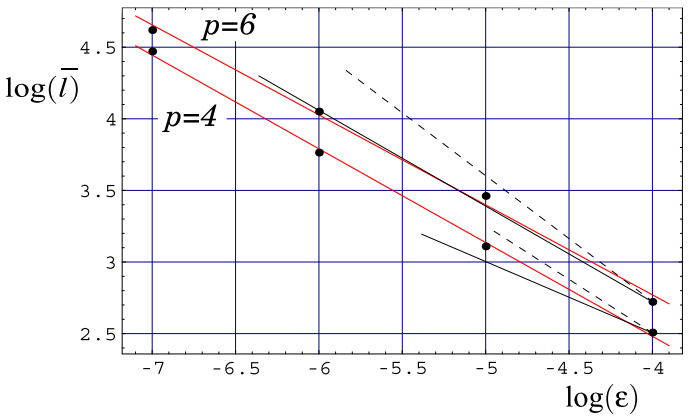

Fig. 7. Characteristic relations for the map (24) for the two cases of Fig. 2 with $\hat{x} = -0.05$. Dots stand for numerical data. The solid black segments slopes are given by Eq. (22) for $p = 4$ and $p = 6$. Dashed black segments are the same as above, but with slopes given by Eq. (23). Red solid lines show the least mean square fitting of the numerical data, giving $\beta_{p=6} = 0.63$ close to $\beta = 2/3$, as predicted by Eq. (22), and $\beta_{p=4} = 0.65$, between $\beta = 3/4$ and $\beta = 1/2$ as predicted by Eqs. (22) and (23) respectively. (For interpretation of the references to color in this figure legend, the reader is referred to the web version of this article.)

and the red solid straight lines show the least mean square fitting of the numerical data sets. To support the applicability of Eqs. (22) and (23) in any case, we show in Fig. 7 two line segments with their end points corresponding to the largest ε. These solid line segments have the slope given by Eq. (22) for $p = 6$ and $p = 4$. In the same graph we present the dashed segments corresponding to have used Eq. (23). It is important to note that when $\alpha > 1$ ($p = 6$ in our case) there are not many reinjected points on the left side of $x = 0$. The estimations provided by Eq. (22) are very close to the straight line obtained by fitting the numerical data. Note, however, that for $0 < \alpha < 1$ ($p = 4$ in our case) the straight line fit lies between the lines corresponding to Eqs. (22) and (23). The classical case related to $\alpha < 0$, having many points reinjected on the side $x < 0$, has not been plotted because it is well known and accepted that it fits better in the curve given by Eq. (23).

6. Conclusions

In this work we have extended to Type-I intermittency some recent results obtained in [17,18] to study types I and II intermittencies. Even though, there are many papers devoted to this type of intermittency, to our knowledge, the characterisation of Type-I intermittency based on the characteristic exponent and the probability density $\psi(l)$ of laminar phase length has not been fully considered in its general form, up to now. To study this kind of intermittency by finding $\psi(l)$, we have directly applied the methodology recently developed for the Type-I and Type-III cases [17,18]. We start out our analysis for this work with a numerical evaluation of the function $M(x)$ introduced in the second section. It is argued, and checked in practice, that this function is much more easy to be computed than the reinjection probability density RPD itself. Once $M(x)$ is known, the reinjection probability density can be obtained. This RPD can behave as an increasing or a decreasing function, this is to say, both increasing and decreasing forms may appear. We have found a rich variety of possible profiles for the function $\psi(l)$. Furthermore, for some cases, these $\psi(l)$ shapes are qualitatively different from the classical one. This fact allows us to identify Type-I intermittency cases that might have been hidden until now. We have ascertained a very good agreement between the RPDs and the new analytical probability density $\psi(l)$ of the laminar length with the numerical simulations.

An interesting result we have established states that, in the case of LBR close to zero, the characteristic relation also holds for increasing RPDs. Therefore, we have also shown that very different RPDs can lead to the same characteristic exponent β. The analytical predictions have been supported by several numerical simulations and computational checks. For negative LBR, two limit cases for the characteristic exponent have been addressed. In the first case, when the RPD is an increasing and convex function, the characteristic exponent is obtained by setting $\alpha = 0$ in the general expression Eq. (21) with β given by Eq. (22). On the other hand, the second case can be applied for decreasing RPD and the characteristic exponent is approximated by setting $\alpha = -1$ in Eq. (21), from which the classical expression Eq. (23) is recovered. In either case, the accuracy depends on the LBR value, a fact that demands future research to ensure a more precise description.

Acknowledgements

This work has been supported by the Spanish Ministry of Science and Innovation under Project FIS2010-20054 and the project ISIC/2012/011 (SPACE-CV Generalitat Valenciana Spain), by the CONICET under Project PIP 11220090100809, and by grants of the National University of Córdoba and MCyT of Córdoba, Argentina.

References

[1] Manneville P, Pomeau Y. Intermittency and the Lorenz model. Phys Lett A 1979;75:1–2.
[2] Pomeau Y, Manneville P. Intermittent transition to turbulence in dissipative dynamical systems. Commun Math Phys 1980;74:189–97.
[3] del Rio E, Velarde MG, Rodríguez-Lozano A. Long time data series and difficulties with the characterization of chaotic attractors: a case with intermitency III. Chaos Solitons Fract 1994;4:2169–79.
[4] Stavrinides SG, Miliou AN, Laopoulos Th, Anagnostopoulos AN. The intermittercy route to chaos of an electronic digital oscillator. Int J Bifurcation Chaos 2008;18:1561–6.
[5] Dubois M, Rubio M, Berge P. Experimental evidence of intermittencies associated with a subharmonic bifurcation. Phys Rev Lett 1983;51:1446–9.
[6] Chiriac S, Dimitriu DG, Sandulovicіu M. Type I intermittency related to the spatiotemporal dynamics of double layers and ion-acoustic instabilities in plasma. Phys Plasmas 2007;14:072309.
[7] Stan Cristina, Cristescu CP, Dimitriu DG. Analysis of the intermittent behavior in a low-temperature discharge plasma by recurrence plot quantification. Phys Plasmas 2010;17:042115.
[8] Schuster H, Just W. Deterministic Chaos: An Introduction. Weinheim, Germany: WILEY-VCH Verlag GmbH & Co. KGaA; 2005.
[9] Zebrowski J, Baranowski R. Type I intermittency in nonstationary systems models and human heart rate variability. Physica A 2004;336:74–83.
[10] Chian A. Complex systems approach to economic dynamics. Lecture notes in economics and mathematical systems, 592. Berlin Heidelberg: Springer; 2007. p. 39–50.
[11] Manneville P. Intermittency, self-similarity and 1/f spectrum in dissipative dynamical systems. J Physique 1980;41:1235–43.
[12] Cho JH, Ko MS, Park YJ, Kim CM. Experimental observation of the characteristic relations of Type-I intermittency in the presence of noise. Phys Rev E 2002;65:036222.
[13] Kim CM, Kwon OJ, Lee Eok-Kyun, Lee Hoyun. New characteristic relations in Type-I intermittency. Phys Rev Lett 1994;73:525–8.
[14] Kwon OJ, Kim CM, Lee EK, Lee H. Effects of reinjection on the scaling property of intermittency. Phys Rev E 1996;53:1253–6.
[15] Hirsch JE, Huberman BA, Scalapino DJ. Theory of intermittency. Phys Rev A 1982;25:519–32.
[16] Klimaszewska K, Zebrowski JJ. Detection of the type of intermittency using characteristic patterns in recurrence plots. Phys Rev E 2009;80:026214.
[17] del Rio E, Elaskar S. New characteristic relations in Type-II intermittency. Int J Bifurcation Chaos 2010;20:1185–91.
[18] Elaskar S, del Rio E, Donoso JM. Reinjection probability density in Type-III intermittency. Physica A 2011;390:2759–68.
[19] del Rio Ezequiel, Sanjuán Miguel AF, Elaskar Sergio. Effect of noise on the reinjection probability density in intermittency. Commun Nonlinear Sci Numer Simul 2012;17:3587–96.

[20] Lichtenberg AJ, Lieberman MA. Regular and stochastic motion. New York: Springer-Verlag; 1983.
[21] Abramowitz M, Stegun IA. Handbook of mathematical functions. USA: Dover; 1970.
[22] Bussac MN, Meunier C. Statistical properties of type I intermittency. J Physique 1982;43:585–9.
[23] Honda Katsuya, Kodama Hiroya, Sato Shinichi. Statistical mechanics and crossover scaling for Pomeau–Manneville type intermittent chaos. Phys Lett A 1990;149:101–4.